Microglial-oligodendrocyte interactions in myelination and neurological function recovery after traumatic brain injury

Shanshan Song
University of Pittsburgh
Md Nabiul Hasan
University of Pittsburgh
Lauren Yu
University of Pittsburgh
Satya S. Paruchuri
University of Pittsburgh
John P. Bielanin
University of Pittsburgh
Shamseldin Metwally
University of Pittsburgh
Sydney G. Fischer
University of Pittsburgh
Victoria M. Fiesler
University of Pittsburgh
Tanusree Sen
University of Pittsburgh
Rajaneesh K. Gupta
University of Pittsburgh
Lesley M. Foley
University of Pittsburgh
T. Kevin Hitchens
University of Pittsburgh
C. Edward Dixon
University of Pittsburgh
Franca Cambi
University of Pittsburgh
Nilkantha Sen
University of Pittsburgh
Dandan Sun (sund@upmc.edu)

University of Pittsburgh

Research Article

Keywords: white matter damage, inflammation, oligodendrocytes, microglia, Na+/H+ exchanger, traumatic brain injury

Posted Date: June 28th, 2022

DOI: https://doi.org/10.21203/rs.3.rs-1790060/v1

Abstract

Differential microglial inflammatory responses play a role in regulation of differentiation and maturation of oligodendrocytes (OLs) in brain white matter. How microglia-OL crosstalk is altered by traumatic brain injury (TBI) and its impact on axonal myelination and neurological function impairment remain poorly understood. In this study, we investigated roles of a Na^+/H^+ exchanger (NHE1), an essential microglial pH regulatory protein, in microglial proinflammatory activation and OL survival and differentiation in a murine TBI model induced by controlled cortical impact. Similar TBI-induced contusion volumes were detected in the *Cx3cr1-Cre^{ERT2}* control (Ctrl) mice and selective microglial *Nhe1* knockout (*Cx3cr1-Cre^{ERT2};Nhe1$^{flox/flox}$*, *Nhe1* cKO) mice. Compared to the Ctrl mice, the *Nhe1* cKO mice displayed increased resistance to initial TBI-induced white matter damage and accelerated chronic phase of OL regeneration at 30 d post-TBI. The cKO brains presented increased anti-inflammatory phenotypes of microglia and infiltrated myeloid cells, with reduced proinflammatory transcriptome profiles. Moreover, the cKO mice exhibited accelerated post-TBI sensorimotor and cognitive functional recovery than the Ctrl mice. These phenotypic outcomes in cKO mice were recapitulated in C57BL6J wild-type TBI mice received treatment of a potent NHE1 inhibitor HOE642 for 1-7 days post-TBI. Taken together, these findings collectively demonstrated that blocking NHE1 protein stimulates restorative microglial activation and oligodendrogenesis, which contributes to accelerated white matter repair and neurological function recovery after TBI.

Background

Traumatic brain injury (TBI) causes acute apoptotic death of mature oligodendrocytes (OLs) in the white matter tracts (1), which contributes to prolonged cognitive (2, 3), perceptual (4), and sensorimotor deficits (5). Despite recruitment and accumulation of oligodendrocyte progenitor cells (OPCs) to the injury site from day 2 to 3 months post-injury (1) in white matter repair (6), remyelination mediated by this process is inefficient and often fails due to inadequate OPC differentiation (7), causing sustained axonal demyelination in TBI patients up to 5 years post-TBI (8). To date, no effective treatments are currently available to reduce TBI-induced OL death and/or to stimulate OPC differentiation for white matter repair. A better understanding of the underlying mechanisms of TBI-mediated white matter injury and the identification of new therapeutic targets to stimulate remyelination are warranted. Reducing OL death and white matter damages while promoting differentiation of OPCs into mature myelinating OLs emerge as a central strategy for improving white matter repair and neurological function recovery after TBI.

Microglia play an important role in supporting normal myelin genesis during development and adulthood, as depletion of microglia either in early postnatal stage or in adulthood significantly reduced OPC/OL numbers and inhibited myelin formation in the corpus callosum (CC) and white matter regions of cerebellum (9). Restorative phenotype activation of microglia increases secretion of restorative cytokines/growth factors (TGF-β, IL-10, BDNF, GDNF) and clearing of tissue debris through phagocytosis, which stimulates OL genesis and differentiation for remyelination and brain functional recovery (10, 11). However, activation of microglial inflammation causes secondary damage, which can directly trigger OL

apoptosis and hinder OPC maturation, prolonging post-TBI demyelination (10, 11). Thus, maintaining a balanced microglial activation phenotype homeostasis is important for OL survival, differentiation, and myelination (12).

We recently discovered that activation of microglial NHE1 protein, which mediates H^+ efflux in exchange of Na^+ influx, maintains the optimal alkaline intracellular pH (pH_i) for sustained activation of NADPH oxidase (NOX2) and cytokine release in proinflammatory microglia (13, 14). However, whether microglial NHE1 protein plays a role in regulating microglia-mediated inflammation and microglia-OL interactions after TBI has not been investigated. In this study, we found that either selective deletion of microglial *Nhe1* in the *Cx3cr1-Cre^{ERT2}*;*Nhe1$^{flox/flox}$* (*Nhe1* cKO) mice or pharmacological inhibition of NHE1 protein with its potent inhibitor HOE642 accelerated post-TBI functional recovery, in comparison to the *Cx3cr1-Cre^{ERT2}* control (Ctrl) or vehicle-treated wild-type (WT) mice. The cKO mice not only exhibited increased tolerance to acute post-TBI white matter damage, but also showed accelerated regeneration of the OLs and white matter remyelination at chronic phase post-TBI. Flow cytometry and bulk RNAseq of microglia/macrophages revealed reduced inflammatory responses and increased restorative phenotypes in the cKO brains. Taken together, our findings strongly suggest that targeting NHE1 protein emerges as a novel therapeutic strategy for modulating restorative microglial activation and enhancing oligodendrogenesis in post-TBI white matter repair and neurological function recovery.

Material And Methods

Animals

All animal studies were approved by the University of Pittsburgh Institutional Animal Care and Use Committee, which adhere to the National Institutes of Health Guide for the Care and Use of Laboratory Animals and reported in accordance with the Animal Research: Reporting In Vivo Experiments (ARRIVE) guidelines (15). Tamoxifen-injected *Cx3cr1-Cre$^{ER+/-}$*;*Nhe1$^{flox/flox}$* mice and *Cx3cr1-Cre$^{ER+/-}$* mice were used as cKO and Ctrl groups, as we recently described (16). For the inhibitor study, a potent NHE1 inhibitor HOE642 (Sigma-Aldrich, USA) was administered twice per day by i.p. injections from day 1–7 post-TBI in C57BL/6 male mice, as described in **Supplemental Materials**.

Controlled cortical impact (CCI)-induced TBI procedures

Mice were anesthetized and subjected to CCI as described (17). Briefly, mice were placed in a stereotaxic frame (Leica, Germany) and impacted at 4.5 m/s with 20 ms dwell time and 1.2 mm depression, mimicking a moderate TBI. Sham animals underwent the same procedures without the impact, as described in **Supplemental Materials**.

Behavioral function tests

Neurological functional deficits in mice were screened in a blinded manner with adhesive contact/removal test, foot fault test, and y-maze test, all considered reliable for identifying and

quantifying sensorimotor and cognitive deficits in mouse models of TBI (18–20). Please see **Supplemental Materials** for detailed information.

MRI and DTI of ex vivo brains

At 30 days post-TBI, the same cohort of mice from the behavioral assessments were transcardially perfused with 4% paraformaldehyde (PFA), and *ex vivo* brains were collected for MRI and diffusion tensor imaging (DTI), as described in **Supplemental Materials**. Corpus callosum (CC) and external capsules (EC) were drawn in contralateral (CL) and ipsilateral (IL) hemispheres and values of fractional anisotropy (FA) were calculated, as described before (21).

Flow cytometry profiling of microglia/macrophages

Single cell suspensions were obtained from CL and IL hemispheric tissues using a neural tissue dissociation kit with the gentleMAC Octo Dissociator (Miltenyi Biotech Inc., Germany), as described before (16, 21). Cells were stained with antibodies listed in the **Supplemental Materials.** Data were acquired using an LSRII flow cytometer (BD Biosciences, USA) and analyzed with Flow Jo (Tree Star Inc, USA) software.

Magnetic-activated cell sorting (MACS) isolation of microglia/macrophages

$CD11b^+$ microglia/macrophages were isolated from CL and IL single cell suspensions by MACS using the CD11b MicroBeads (Miltenyi Biotech, USA). Detailed information was described in **Supplemental Materials**.

Bulk RNA sequencing and bioinformatics analysis

Bulk RNA sequencing was performed in MACS-isolated $CD11b^+$ microglia/macrophages and paired-end sequenced on Illumina NovaSeq platform using a Smart Seq v4 library preparation kit, as in our recent report (22). Bioinformatic analysis was performed using Partek Flow 8.0 software (Partek, USA), as described in **Supplemental Materials**. The sequencing data have been deposited to the Gene Expression Omnibus (GEO) database with experiment series accession number GSE199869.

Quantitative real-time PCR

RNA was isolated from the MACS-isolated $CD11b^+$ microglia/macrophages using a Direct-zol RNA MicroPrep Kit (Zymo Research, USA), following the manufacturer's instruction. qPCR was performed on a CFX96 Real-Time PCR Detection System (Bio-rad, USA), as described in **Supplemental Materials**. Data were analyzed using the ΔΔCt method (23) with triplicate reactions for each gene evaluated. Primer sequences are listed in **Supplementary Table S1**.

Immunofluorescent staining

Mouse brains were fixed with transcardial perfusion with 4% PFA, and cryosectioned at 25 μm thickness for immunofluorescent staining, as described in **Supplemental Materials**. Identical acquisition parameters

were used and fluorescent images were obtained using a Nikon A1R confocal microscope (Nikon, Japan) before analyzing with ImageJ (NIH, USA).

Statistical analysis

Unbiased study design and analyses were used in all the experiments. Blinding of investigators to experimental groups were maintained until data were fully analyzed whenever possible. Power analysis were performed based on the mean and variability of data from our laboratory. N = 8 mice/group for behavioral tests, N = 6 for immunostaining, flow cytometry, qPCR, and N = 4 for RNAseq and MRI/DTI were sufficient to give us 80% power to detect 20% changes with 0.05 two-sided significance. Data were expressed as mean ± SEM. Two-tailed Student's t-test with 95% confidence was used when comparing two conditions. For more than two conditions, two-way ANOVA analysis was used. P value < 0.05 was considered statistically significant (Prism, GraphPad, USA).

Results

Microglial Nhe1 **cKO mice exhibited accelerated sensorimotor and cognitive function recovery after TBI**

We demonstrated in our recent report that our *Nhe1* cKO mouse line successfully deleted NHE1 protein expression exclusively in the IBA1$^+$ microglia/macrophages, but remained unchanged in other cell types (21). Survival rate and neurological behavior functions in Ctrl and *Nhe1* cKO mice were monitored during 1–30 days post-TBI (Fig. 1a). Neither Sham Ctrl or Sham cKO mice displayed any mortality, while Ctrl and cKO TBI mice exhibited < 10% mortality (Fig. 1b). Ctrl and cKO TBI mice showed similar contusion volume initially at 3 days post-TBI (Fig. 1c). However, the unbiased analysis of NeuN$^+$ neuronal counts by automatic cell counting (using the "count particles" module in ImageJ) revealed significantly higher NeuN$^+$ cell percentages in both CL and IL peri-lesion areas of the cKO brains than the Ctrl brains (Fig. 1d). In neurological behavioral assessments, Ctrl and cKO sham animals similarly showed a brief elevation of sensorimotor deficits at 1 day post-sham, but quickly returned to baseline at 3 days post-procedure (Fig. 1e-f). In comparison, the Ctrl TBI mice exhibited significantly prolonged contact and removal time (~ 20-fold and 10-fold, respectively), as well as significantly more errors in the foot fault test (~ 4-fold) at 1–7 days post-TBI (Fig. 1e-f). However, compared to the Ctrl TBI mice, the *Nhe1* cKO mice showed significantly accelerated sensorimotor function recovery during 5–14 days post-TBI, and completely returned to their baseline levels by day 14 (Fig. 1e-f). In testing working memory using the Y-maze test at 30 days post-TBI, the cKO mice exhibited a significantly higher spontaneous alternation rate (~ 73%) than the Ctrl mice (~ 46%, $p < 0.0001$), indicating a stimulated working memory function in the cKO mice (Fig. 1g). However, the two groups displayed similar locomotor activities reflected by total arm entries (**Fig. S1a**). Taken together, these neurological function assessment tests demonstrate that the *Nhe1* cKO mice exhibited better neurological function (sensorimotor and cognitive) recovery after TBI.

Microglial Nhe1 **cKO mice displayed improved white matter resistance against TBI-induced apoptosis and inhibition of oligodendrogenesis**

As white matter integrity is important for restoring neurological functions after TBI (2, 8), we tested whether the improved functional outcomes of the cKO mice were in part due to their increased tolerance to TBI-induced damage and/or boosted white matter repair. Myelin basic protein (MBP), a marker for white matter myelination, was used to assess corpus callosum (CC) tract integrity in the Ctrl and cKO brains after sham or TBI procedures. Interestingly, the cKO brains exhibited a thicker CC (midline, same bregma level, **Fig. S2**) at 24 h after sham procedure (Fig. 2a, $p < 0.05$), indicating a possible role of microglial NHE1 protein in regulating white matter integrity homeostasis. At 1 d post-TBI, the cKO brains showed a significantly higher CC thickness than the Ctrl brains (Fig. 2a, $p < 0.001$). Further analysis of $Olig2^+$ oligodendrocyte lineage cells at 3 days post-TBI revealed significantly elevated $NG2^+Olig2^+$ OPCs, $Ki67^+Olig2^+$ proliferative OLs, and reduced $Caspase3^+Olig2^+$ apoptotic OLs in both hemispheres of the cKO brains, compared to Ctrl brains (Fig. 2b, $p < 0.05$). Importantly, these cKO brains also exhibited increased expression of H3K9me3 in the $Olig2^+$ OLs, a post-translational histone modification marker for OPC differentiation (24) (Fig. 2b, $p < 0.01$). Moreover, analysis of APC^+ mature OLs counts showed that TBI did not affect OL survival in the CL hemispheres of either Ctrl or cKO brains, but induced an immediate decrease of the APC^+ mature OLs in the IL hemisphere of the Ctrl mice at 1 d post-TBI (Fig. 2c-e, $p < 0.01$). In contrast, the cKO TBI brains were resistant to such a loss in the IL hemisphere (Fig. 2c-e). The Ctrl TBI mice continued to lose mature OLs in both CL and IL CC at 3 days post-TBI, while the TBI-induced reduction of mature OLs in the cKO CC was delayed (Fig. 2c-e). Interestingly, by 30 days post-TBI, the mature OLs in Ctrl mice failed to regenerate, while the cKO brains exhibited significantly elevated counts of mature OLs in both hemispheres of the CC tracks (Fig. 2e, $p < 0.01$). These findings strongly suggest that deletion of microglial NHE1 protein not only provided resistance to the white matter damage induced by TBI, but also promoted oligodendrogenesis by increasing their progenitor cell proliferation and differentiation into mature myelinating OLs.

Selective deletion of microglial Nhe1 increased microglial anti-inflammatory phenotype activation in TBI brains

To understand the underlying mechanisms of the increased oligodendrogenesis in the post-TBI cKO brains, we examined the profiling of microglia and infiltrated myeloid cells in Ctrl or *Nhe1* cKO brains at 3 days post-TBI with flow cytometry (Fig. 3a). No difference in the percentage of microglial cells ($CD11b^+CD45^{lo}$) and infiltrated myeloid cells ($CD11b^+CD45^{hi}$) were detected in CL or IL hemispheres of the Ctrl and *Nhe1* cKO mice (Fig. 3b, $p > 0.05$). Further probing of the expression of pro-inflammatory markers CD16/32 and CD86 did not show any differences between Ctrl and cKO microglia and/or myeloid cells (Fig. 3c-d). However, the percentage of anti-inflammatory CD206-positive microglia/myeloid cells and Ym-1^{hi}-positive microglia were significantly increased in the IL hemisphere of the cKO brains, compared to the Ctrl (Fig. 3c-d, $p < 0.05$). Further characterization of microglial cells or reactive astrocytes in the peri-lesion cortex of Ctrl or cKO brains by immunofluorescent staining revealed that TBI induced significant increases in $GFAP^+$ astrocytes and $IBA1^+$ microglia/macrophage counts in both the Ctrl and cKO brains at 3 days post-TBI (Fig. 3e, $p < 0.05$), but, the cKO brains showed significantly attenuated $GFAP^+$ astrocyte and IBA^+ microglia/macrophage counts were significantly attenuated in the peri-lesion

area of the cKO brains, compared to the Ctrl (Fig. 3e, $p < 0.001$). Taken together, these findings demonstrate that selective deletion of microglial *Nhe1* gene promotes the restorative activation of microglia/myeloid cells and reduces astrogliosis in the cKO brains.

Selective deletion of microglial Nhe1 altered inflammation-related transcriptome profile in microglia/macrophages after TBI

To understand how deletion of microglial *Nhe1* affects microglial restorative function, we performed bulk RNA sequencing (RNA-seq) of $CD11b^+$ cells isolated from the CL and IL hemispheres of Ctrl and *Nhe1* cKO brains at 3 days post-TBI (Fig. 4a). Unsupervised hierarchical clustering analysis demonstrated clear separation between CL and IL hemispheres of cKO and Ctrl brains (Fig. 4b). 123 differentially expressed genes (DEGs) were identified in the IL hemispheres of cKO mice, compared to Ctrl mice (fold change ≥ 1.2 or ≤ -1.2 and FDR q-value ≤ 0.05, Fig. 4c); among those, 56 genes were upregulated and 67 downregulated (Fig. 4d). Ingenuity Pathway Analysis (IPA) showed significantly altered enrichment pathways, including Th1 and Th2 activation pathways (Fig. 4e, $p < 0.05$), which is known to elicit inflammation in microglia and macrophages (25). Within these pathways, multiple pro-inflammatory genes were triggered by TBI in the Ctrl microglia/macrophages, but significantly decreased in the cKO microglia/macrophages, such as *Psen2*, *Ifi206*, *Ifi207*, and *Igsf8* (Fig. 4d, f), all reported to be involved in microglia/macrophage-mediated inflammation (26–29). *S1pr1* and *Tpm3* genes are also involved in inflammation and expression of these two genes were reduced significantly in cKO IL hemisphere compared to ctrl IL hemisphere (Fig. 4f). Additionally, the cKO microglia/macrophages showed elevated expressions of *Fcgr1*, *Gnb4*, and *B4galnt1* genes which stimulate anti-inflammatory activation (28, 30). On the other hand, the non-lesion CL hemispheres displayed 178 DEGs between Ctrl and cKO microglia/macrophages (**Fig. S3a-b**), with IPA analysis showing significantly altered IL-8 signaling pathway with reduced inflammatory genes such as *Napepld*, *Vcam1*, *Rnd1* (31) in the cKO microglia/macrophages (**Fig. S3b-d**). Change of selected key pathway genes have been validated by qRT-PCR (**Fig. S4**). Taken together, our bioinformatic analysis reveals that deletion of microglial *Nhe1* attenuates the expression of inflammation-related transcriptomes but stimulates restorative microglial activation transcriptome profiles after TBI.

Post-TBI administration of selective NHE1 inhibitor HOE642 accelerated neurological function recovery

We next explored the efficacy of targeting NHE1 protein with a pharmacological inhibition approach in reducing the TBI-induced functional deficits. Figure 5a illustrated our administration protocol of Veh (DMSO) or a potent NHE1 inhibitor HOE642 (0.3 mg/kg body weight/day, twice per day, i.p.) at 24 h post-TBI. Compared to the Veh-treated TBI mice, HOE642 administration did not affect mortality during 30 days post-TBI (Fig. 5b). However, the HOE642-treated TBI mice exhibited significant improvements in sensorimotor function (adhesive contact/removal test and foot fault test) during the 14 days post-TBI recovery period (Fig. 5c-d, $p < 0.05$). In assessing the same cohort of mice in cognitive function with Y-maze test at 30 days post-TBI, the HOE642-treated mice exhibited an improved trend of performance in

spontaneous alternation rate than the Veh-treated mice (Fig. 5e, $p = 0.09$), indicating improved working memory function (32). These HOE-treated TBI mice also showed significantly increased locomotor activity reflected by their total arm entries (Fig. 5e, $p < 0.05$). These outcomes are consistent with the *Nhe1* cKO mice shown in Fig. 1.

Characterization of the HOE642-mediated protective effects in TBI mice

Compared to the Veh-treated mice, the HOE-treated mice exhibited significantly smaller contusion volume and increased $NeuN^+$ neurons at 3 days post-TBI (both CL and IL peri-lesion areas) (Fig. 6a-b, $p < 0.05$), indicating that post-TBI administration of HOE642 has neuroprotective effects. In line with the boosted white matter repair in the *Nhe1* cKO mice, the HOE-treated brains showed increased oligodendrogenesis and differentiation properties in the CC white matter tracts compared to the Veh-treated brains at 3 days post-TBI (Fig. 6c, $p < 0.05$). Moreover, flow cytometry of $CD11b^+CD45^{lo}$ microglia and $CD11b^+CD45^{hi}$ myeloid cells from the Veh or HOE-treated brains (**Fig. S5a-b**) showed that the anti-inflammatory phenotype ($CD206^+$) of microglia cells were selectively increased in the IL hemisphere of the HOE-treated brains (**Fig. S5c**, $p < 0.05$), while sparing the pro-inflammatory phenotypes of myeloid cells or microglial cells (**Fig. S5c-d**). Immunostaining further confirmed that $IBA1^+$ microglia/macrophages and $GFAP^+$ reactive astrocytes were significantly reduced in the peri-lesion cortex of HOE-treated brains (**Fig. S5e**, $p < 0.0001$). These findings collectively suggest that post-TBI administration of NHE1 protein inhibitor HOE642 is protective of neurons and reduced inflammatory responses and gliosis in the brain, which can concertedly contribute to the improved functional outcome post-TBI.

Long-term effects of NHE1 protein blockade on white matter integrity after TBI

We further assessed whether the *Nhe1* cKO brains and HOE-treated brains exhibited long-lasting preservation of white matter integrity by 30 days post-TBI via MRI DTI of the *ex vivo* brains of the same cohort of mice after completing neurological function testing. The cKO mice exhibited significantly reduced brain lesion volume at 30 days post-TBI, compared to the Ctrl mice (Fig. 7a-b). Interestingly, both the *Nhe1* cKO brains and HOE-treated brains displayed increased FA values in the CC and EC white matter tracts (both hemispheres) by 30 days post-TBI, compared to either Ctrl or Veh-treated brains (Fig. 7c, $p < 0.05$). Additionally, white matter demyelination is associated with higher radial diffusivity (RD) and medial diffusivity (MD), but not necessarily with reduced axial diffusivity (AD) (33, 34). We indeed detected lower RD and MD, but higher AD in the same cohort of either cKO or HOE-treated mice **(Fig. S6).** Taken together, these data collectively demonstrate that blocking microglial NHE1 protein has sustained long-term protective effects on white matter myelination, and reveals NHE1 protein as a potential therapeutic target for white matter repair after TBI.

Discussion

Clinical studies showed that sustained demyelination and loss of mature OLs in CC and EC white matter tracts can be detected as early as 10 hrs-2 weeks post-TBI (35), and that these changes can persist up to 5 years after TBI, which play a causative role in developing chronic cognitive functional deficit post-TBI (8). TBI triggers potent neuroinflammatory reactions in the brain, mediated by a complex cascade of cellular and molecular events (36), including excessive glutamate release, rapid depletion of ATP, increased oxidative stress, and elevated inflammation, altogether contributing to the loss of myelin sheath, OLs death, and inhibition of OL maturation after TBI (1, 7, 37). Within minutes after TBI, microglia become activated, releasing proinflammatory cytokines (IFN-γ, TNF-α, IL-1β), reactive oxygen species (ROS), and inflammasome (such as NLRP3)-containing extracellular vesicles, etc., which exacerbate injury (38–40). However, microglia are highly plastic cells and can also respond to cytokines released by Th2 cells in the surrounding environment, such as IL-4 and IL-13, to promote an alternative state phenotype that is associated with growth and tissue repair (36). Thus, the alternatively activated microglial cells can provide neuroprotective qualities, such as oligodendrogenesis, angiogenesis, and remyelination, following injury post-TBI (40). Regulating microglial phenotypic conversion to minimize the neurotoxic events, while preserving the neuroprotective qualities, emerges as a novel strategy in developing new treatments for minimizing white matter damage and promoting remyelination in TBI patients.

Microglia play an important role in supporting normal myelinogenesis during development and adulthood, with distinctly high expression of a lysosomal marker LAMP2, as well as upregulated genes such as *Spp1, Gpnmb, Igf1*, as well as the ATPase H^+ transporting V0 Subunit D2 gene *Atp6v0d2* (9). We previously reported that NHE1 protein, which mediates H^+ efflux in exchange of Na^+ influx, is essential in regulating microglial homeostatic pH_i (13), similar to the roles of the ATPase H^+ pump in myelin-supporting microglia (9). Upon brain injury, NHE1 protein is rapidly activated and mediates H^+ extrusion activity to maintain the optimal alkaline microglial pH_i for NADPH oxidase (NOX) activation, ROS production, and inflammation (Fig. 8) (13, 14). In the current study, blocking NHE1 protein activity, either by genetic deletion or pharmacological inhibition, reduced the microglial pro-inflammatory phenotype and increased the anti-inflammatory profiling during the acute phase after TBI (Fig. 8) where early activation of the restorative phenotype is proven to be essential in long-term tissue repair and functional recovery after TBI (38). Regarding the significantly higher spontaneous alternation rate in the post-TBI cKO mice compared to their sham controls, we recently showed that the cKO mice exhibited increased microglial phagocytosis and improved synaptic remodeling after ischemic stroke, compared to their sham control mice (16). We suspect that similar mechanisms may play a role in these post-TBI mice as well. The transition of microglial functions from detrimental to restorative is essential in the initiation of OPC differentiation and the start of remyelination in a demyelination model (41) as well as in stroke (42). In both microglia-specific *Nhe1* cKO mice and HOE642-treated WT mice post-TBI, we detected increased anti-inflammatory phenotype of microglia and enhanced white matter myelination and oligodendrogenesis (Fig. 8). This is corroborated by our RNAseq analysis which revealed significantly reduced proinflammatory pathways in the cKO microglia, compared to the Ctrl microglia. These changes could concertedly enhance the proliferation and differentiation of the OL/OPCs, and result in improved

white matter repair, which underlies the accelerated functional recovery after TBI. In terms of neuroprotection, the cKO brains showed significantly increased percentage of $NeuN^+$ neurons within total cells in the cKO brains (Fig. 1d), without significant improvement for lesion volume or absolute $NeuN^+$ counts (Fig. 1c-d, **Fig. S7a**). On the other hand, compared to the Veh-treated brains, HOE treatment significantly increased both absolute cell counts and percentage of $NeuN^+$ cells in the perilesion area (**Fig. S7b**). These results could be confounded by the total cell numbers in the area (**Fig. S7a-b**), where infiltrated inflammatory cells play an important role (43). The significantly reduced $NeuN^-$ cells (**Fig. S7a-b**) along with the increased $GFAP^+$ astrocytes and $IBA1^+$ microglia in the perilesion areas of either cKO or HOE-treated brains (Fig. 3e, **Fig. S5e**) further validated this speculation.

Last but not least, as NHE1 protein is ubiquitously expressed in all cell types in the CNS, the current pharmacological approach is not cell-specific and can affect NHE1 protein function in all cell types. Since pH_i is involved in regulating OL division and their differentiation into mature OLs (44), blocking oligodendrocytic NHE1 via HOE642 could also regulate pH_i in OLs and play a direct role in promoting oligodendrogenesis for post-TBI white matter repair. In addition, HOE642 treatment may block astrocytic NHE1 protein and indirectly modulate microglial function through astrocyte-microglia interactions (45, 46). It was reported that loss of NHE1 protein enhances neuronal excitability and leads to increased occurrence of epilepsy (47). However, we detected neuroprotective effects and significant reduction of contusion volume in the HOE642-treated mice. Thus, future studies are warranted to dissect the protective effects of HOE642 in various cell types after TBI. In addition, since sex-specific differences in male and female microglial functions have been observed after ischemic stroke (48), we disaggregated the data to evaluate for sex-dependent differences after TBI. We observed similar trends of data between males and females in Ctrl or cKO mice (**Fig. S8**), thus we only tested in males for the pharmacological study. Further study may be warranted utilizing both males and females in evaluating the clinical efficacy of HOE642 treatment after TBI.

Conclusion

To date, no treatment was proven effective for reducing white matter damage and/or stimulating white matter remyelination after TBI. Our findings demonstrate that blockade of NHE1 protein activity, either by genetic deletion or pharmacological approach, accelerated post-TBI neurological functional recovery by reducing microglial inflammatory activation, neurodegeneration, and stimulating oligodendrogenesis in white matter repair (Fig. 8). We identified NHE1 protein as a potential therapeutic target for post-TBI white matter repair and functional improvement.

Abbreviations

ARRIVE Animal Research: Reporting In Vivo Experiments

AD Axial diffusivity

CL	Contralateral
Ctrl	Control
CC	Corpus callosum
DEG	Differentially expressed gene
DTI	Diffusion tensor imaging
EC	External capsules
FA	Fractional anisotropy
GEO	Gene Expression Omnibus
IPA	Ingenuity Pathway Analysis
IL	Ipsilateral
pH_i	Intracellular pH
MACS	Magnetic-activated cell sorting
MD	Medial diffusivity
cKO	Conditional knockout
MBP	Myelin basic protein
NHE1	Na^+/H^+ exchanger isoform-1
NOX	NADPH oxidase
OL	Oligodendrocytes
OPC	Oligodendrocyte progenitor cells
PFA	Paraformaldehyde
RD	Radial diffusivity
RNA-seq	RNA sequencing
TBI	Traumatic brain injury

WT	Wild-type

Declarations

Ethics approval and consent to participate

All animal studies were approved by the University of Pittsburgh Medical Center Institutional Animal Care and Use Committee, which adhere to the National Institutes of Health Guide for the Care and Use of Laboratory Animals and reported in accordance with the Animal Research: Reporting In Vivo Experiments (ARRIVE) guidelines (15).

Consent for publication

Not applicable.

Availability of data and materials

All the data associated with this study are present in the paper or the Supplementary Materials. The RNA sequencing data have been deposited to the Gene Expression Omnibus database with experiment series accession number GSE199869.

Competing interests

The authors have no competing interests to declare.

Funding

This study was funded by Veterans Affairs Merit Award I01 BX004625 (Sun) and Career Research Scientist award IK6BX005647 (Sun).

Authors' contributions

DS designed and supervised the project; SS, MNH, LY, SSP, JPB, SM, SGF, VMF, TS, RKG, LMF, TKH performed research and SS, MNH, LY, SSP, RKG performed data analysis; SS, MNH, LY, SSP, JPB, LMF, TKH, CED, FC, NS, and DS wrote, edited, and proofread the manuscript. All authors contributed to the article and approved the submitted version. All authors read and approved the final manuscript.

Acknowledgements

We thank the Molecular Biology Information Service of the Health Sciences Library System at the University of Pittsburgh to provide licenses for Partek Flow and Ingenuity Pathway Analysis software, and the University of Pittsburgh Center for Research Computing (CRC) for the resources in conducting the RNAseq analysis.

References

1. Dent KA, Christie KJ, Bye N, Basrai HS, Turbic A, Habgood M, et al. Oligodendrocyte birth and death following traumatic brain injury in adult mice. PLoS One. 2015;10(3):e0121541.
2. Croall ID, Cowie CJ, He J, Peel A, Wood J, Aribisala BS, et al. White matter correlates of cognitive dysfunction after mild traumatic brain injury. Neurology. 2014;83(6):494–501.
3. Taib T, Leconte C, Van Steenwinckel J, Cho AH, Palmier B, Torsello E, et al. Neuroinflammation, myelin and behavior: Temporal patterns following mild traumatic brain injury in mice. PLoS One. 2017;12(9):e0184811.
4. Vaessen MJ, Saj A, Lovblad KO, Gschwind M, Vuilleumier P. Structural white-matter connections mediating distinct behavioral components of spatial neglect in right brain-damaged patients. Cortex. 2016;77:54–68.
5. Corbetta M, Ramsey L, Callejas A, Baldassarre A, Hacker CD, Siegel JS, et al. Common behavioral clusters and subcortical anatomy in stroke. Neuron. 2015;85(5):927–41.
6. Flygt J, Clausen F, Marklund N. Diffuse traumatic brain injury in the mouse induces a transient proliferation of oligodendrocyte progenitor cells in injured white matter tracts. Restor Neurol Neurosci. 2017;35(2):251–63.
7. Huntemer-Silveira A, Patil N, Brickner MA, Parr AM. Strategies for Oligodendrocyte and Myelin Repair in Traumatic CNS Injury. Front Cell Neurosci. 2020;14:619707.
8. Dinkel J, Drier A, Khalilzadeh O, Perlbarg V, Czernecki V, Gupta R, et al. Long-term white matter changes after severe traumatic brain injury: a 5-year prospective cohort. AJNR Am J Neuroradiol. 2014;35(1):23–9.
9. Hagemeyer N, Hanft KM, Akriditou MA, Unger N, Park ES, Stanley ER, et al. Microglia contribute to normal myelinogenesis and to oligodendrocyte progenitor maintenance during adulthood. Acta Neuropathol. 2017;134(3):441–58.
10. Shi H, Hu X, Leak RK, Shi Y, An C, Suenaga J, et al. Demyelination as a rational therapeutic target for ischemic or traumatic brain injury. Exp Neurol. 2015;272:17–25.
11. Mira RG, Lira M, Cerpa W. Traumatic Brain Injury: Mechanisms of Glial Response. Front Physiol. 2021;12:740939.
12. Miron VE. Microglia-driven regulation of oligodendrocyte lineage cells, myelination, and remyelination. J Leukoc Biol. 2017;101(5):1103–8.
13. Liu Y, Kintner DB, Chanana V, Algharabli J, Chen X, Gao Y, et al. Activation of microglia depends on Na+/H + exchange-mediated H + homeostasis. J Neurosci. 2010;30(45):15210–20.
14. Lam TI, Brennan-Minnella AM, Won SJ, Shen Y, Hefner C, Shi Y, et al. Intracellular pH reduction prevents excitotoxic and ischemic neuronal death by inhibiting NADPH oxidase. Proc Natl Acad Sci U S A. 2013;110(46):E4362-8.
15. Percie du Sert N, Hurst V, Ahluwalia A, Alam S, Avey MT, Baker M, et al. The ARRIVE guidelines 2.0: Updated guidelines for reporting animal research. J Cereb Blood Flow Metab. 2020;40(9):1769–77.

16. Song S, Yu, L., Hasan, M.N., Paruchuri, S., Mullett, S.J., Sullivan, M.L.G., Fiesler, V.M., Young, C.B., Stolz, D.B., Wendell, S.G., Sun, D. Stimulating microglial oxidative phosphorylation and phagocytosis in post-stroke brain repair and cognitive function recovery. Commun Biol. 2021;in press.
17. Sen T, Gupta R, Kaiser H, Sen N. Activation of PERK Elicits Memory Impairment through Inactivation of CREB and Downregulation of PSD95 After Traumatic Brain Injury. J Neurosci. 2017;37(24):5900–11.
18. Bouet V, Boulouard M, Toutain J, Divoux D, Bernaudin M, Schumann-Bard P, et al. The adhesive removal test: a sensitive method to assess sensorimotor deficits in mice. Nat Protoc. 2009;4(10):1560–4.
19. Shelton SB, Pettigrew DB, Hermann AD, Zhou W, Sullivan PM, Crutcher KA, et al. A simple, efficient tool for assessment of mice after unilateral cortex injury. J Neurosci Methods. 2008;168(2):431–42.
20. Darwish H, Hasan H. Y-Shaped Maze to Test Spontaneous Object Recognition and Temporal Order Memory After Traumatic Brain Injury. Methods Mol Biol. 2019;2011:383–92.
21. Song S, Wang S, Pigott VM, Jiang T, Foley LM, Mishra A, et al. Selective role of Na(+) /H(+) exchanger in Cx3cr1(+) microglial activation, white matter demyelination, and post-stroke function recovery. Glia. 2018;66(11):2279–98.
22. Hasan MN, Luo L, Ding D, Song S, Bhuiyan MIH, Liu R, et al. Blocking NHE1 stimulates glioma tumor immunity by restoring OXPHOS function of myeloid cells. Theranostics. 2021;11(3):1295–309.
23. Livak KJ, Schmittgen TD. Analysis of relative gene expression data using real-time quantitative PCR and the 2(-Delta Delta C(T)) Method. Methods. 2001;25(4):402–8.
24. Gibson EM, Purger D, Mount CW, Goldstein AK, Lin GL, Wood LS, et al. Neuronal activity promotes oligodendrogenesis and adaptive myelination in the mammalian brain. Science. 2014;344(6183):1252304.
25. Abdelaziz MH, Abdelwahab SF, Wan J, Cai W, Huixuan W, Jianjun C, et al. Alternatively activated macrophages; a double-edged sword in allergic asthma. J Transl Med. 2020;18(1):58.
26. Weigert A, Olesch C, Brune B. Sphingosine-1-Phosphate and Macrophage Biology-How the Sphinx Tames the Big Eater. Front Immunol. 2019;10:1706.
27. Mondini M, Costa S, Sponza S, Gugliesi F, Gariglio M, Landolfo S. The interferon-inducible HIN-200 gene family in apoptosis and inflammation: implication for autoimmunity. Autoimmunity. 2010;43(3):226–31.
28. Orecchioni M, Ghosheh Y, Pramod AB, Ley K. Macrophage Polarization: Different Gene Signatures in M1(LPS+) vs. Classically and M2(LPS-) vs. Alternatively Activated Macrophages. Front Immunol. 2019;10:1084.
29. Tian Z, Zhao J, Wang Y. The prognostic value of TPM1-4 in hepatocellular carcinoma. Cancer Med. 2022;11(2):433–46.
30. Palma A, Jarrah AS, Tieri P, Cesareni G, Castiglione F. Gene Regulatory Network Modeling of Macrophage Differentiation Corroborates the Continuum Hypothesis of Polarization States. Front Physiol. 2018;9:1659.

31. Brat DJ, Bellail AC, Van Meir EG. The role of interleukin-8 and its receptors in gliomagenesis and tumoral angiogenesis. Neuro Oncol. 2005;7(2):122–33.
32. Kraeuter AK, Guest PC, Sarnyai Z. The Y-Maze for Assessment of Spatial Working and Reference Memory in Mice. Methods Mol Biol. 2019;1916:105–11.
33. Min ZG, Shan HR, Xu L, Yuan DH, Sheng XX, Xie WC, et al. Diffusion tensor imaging revealed different pathological processes of white matter hyperintensities. BMC Neurol. 2021;21(1):128.
34. Song SK, Sun SW, Ramsbottom MJ, Chang C, Russell J, Cross AH. Dysmyelination revealed through MRI as increased radial (but unchanged axial) diffusion of water. Neuroimage. 2002;17(3):1429–36.
35. Johnson VE, Stewart JE, Begbie FD, Trojanowski JQ, Smith DH, Stewart W. Inflammation and white matter degeneration persist for years after a single traumatic brain injury. Brain. 2013;136(Pt 1):28–42.
36. Loane DJ, Kumar A. Microglia in the TBI brain: The good, the bad, and the dysregulated. Exp Neurol. 2016;275 Pt 3:316 – 27.
37. Ng SY, Lee AYW. Traumatic Brain Injuries: Pathophysiology and Potential Therapeutic Targets. Front Cell Neurosci. 2019;13:528.
38. Donat CK, Scott G, Gentleman SM, Sastre M. Microglial Activation in Traumatic Brain Injury. Front Aging Neurosci. 2017;9:208.
39. Hernandez-Ontiveros DG, Tajiri N, Acosta S, Giunta B, Tan J, Borlongan CV. Microglia activation as a biomarker for traumatic brain injury. Front Neurol. 2013;4:30.
40. Xu H, Wang Z, Li J, Wu H, Peng Y, Fan L, et al. The Polarization States of Microglia in TBI: A New Paradigm for Pharmacological Intervention. Neural Plast. 2017;2017:5405104.
41. Miron VE, Boyd A, Zhao JW, Yuen TJ, Ruckh JM, Shadrach JL, et al. M2 microglia and macrophages drive oligodendrocyte differentiation during CNS remyelination. Nat Neurosci. 2013;16(9):1211–8.
42. Raffaele S, Gelosa P, Bonfanti E, Lombardi M, Castiglioni L, Cimino M, et al. Microglial vesicles improve post-stroke recovery by preventing immune cell senescence and favoring oligodendrogenesis. Mol Ther. 2021;29(4):1439–58.
43. Alam A, Thelin EP, Tajsic T, Khan DZ, Khellaf A, Patani R, et al. Cellular infiltration in traumatic brain injury. J Neuroinflammation. 2020;17(1):328.
44. Boussouf A, Gaillard S. Intracellular pH changes during oligodendrocyte differentiation in primary culture. J Neurosci Res. 2000;59(6):731–9.
45. Ma Y, Wang J, Wang Y, Yang GY. The biphasic function of microglia in ischemic stroke. Prog Neurobiol. 2017;157:247–72.
46. Zhao SC, Ma LS, Chu ZH, Xu H, Wu WQ, Liu F. Regulation of microglial activation in stroke. Acta Pharmacol Sin. 2017;38(4):445–58.
47. Zhao H, Carney KE, Falgoust L, Pan JW, Sun D, Zhang Z. Emerging roles of Na(+)/H(+) exchangers in epilepsy and developmental brain disorders. Prog Neurobiol. 2016;138–140:19–35.

48. Villa A, Gelosa P, Castiglioni L, Cimino M, Rizzi N, Pepe G, et al. Sex-Specific Features of Microglia from Adult Mice. Cell Rep. 2018;23(12):3501–11.

Figures

Figure 1

Effects of microglial *Nhe1* deletion on contusion volume and neurological function recovery in post-TBI mice.

a. Experimental protocol. *Cx3cr1-Cre*$^{ER+/-}$ control (Ctrl) mice or *Cx3cr1-CreE*$^{R+/-}$*;Nhe1*$^{f/f}$ (*Nhe1* cKO) mice at postnatal day 30-40 (P30-40) were given tamoxifen (Tam, 75 mg/kg body weight/day at a concentration of 20 mg/ml in corn oil, intraperitoneally) for five consecutive days. A 30-day post-injection waiting period was used for clearance of Tam and for replenishing of peripheral *Cx3cr1*$^{+}$ monocytes prior to the induction of CCI or sham procedures. **b.** Survival curve of Ctrl and cKO mice during 1-30 days post-sham or TBI. **c.** Contusion volume of Ctrl or cKO brains at 3 days post-TBI assessed by neuronal marker MAP2 expression. **d.** Representative images of neuronal marker MAP2 and NeuN expressions with unbiased automatic quantification of NeuN^{+} neurons in the contralateral (CL) and the ipsilateral (IL) peri-lesion cortex of Ctrl or cKO brains at 3 days post-TBI. N = 5 for Ctrl (3 males, 2 females), and N = 6 for cKO (4 males, 2 females). Scale bar = 50 μm**. e.** Adhesive tape removal test in mice at 1-14 d post-sham or TBI. **f.** Foot fault test in the same cohort of mice as in e. **g.** Y-maze test in the same cohort of mice as in e. Data are mean ± SEM. N = 5 for sham groups, N = 8 for TBI groups (all males). * $p < 0.05$, ** $p < 0.01$, **** $p < 0.0001$, Ctrl TBI vs. cKO TBI. # $p<0.05$, ## $p < 0.01$, ### $p < 0.001$ Ctrl TBI vs. Ctrl sham. $ $p<0.05$, $$ $p<0.01$, cKO TBI vs. cKO sham.

Figure 2

Microglial *Nhe1* cKO mice increased white matter tolerance to TBI with enhanced oligodendrogenesis and differentiation.

a. Representative immunofluorescent images of MBP staining (at same bregma level) showing the cKO mice exhibited increased corpus callosum (CC) thickness at 1 day after sham or CCI procedures. N = 3 for Ctrl sham (1 male, 2 females) and cKO sham (1 male, 2 females); N = 4 for Ctrl TBI (2 males, 2 females) and cKO TBI (2 males, 2 females). Boxed areas indicate locations where zoom-in images (in b and c) were collected. **b.** Representative images and quantification of Olig2 colocalized with NG2, Ki67, Caspase-3, and H3K9me3 in CC of Ctrl or cKO brains at 3 days post-TBI. N = 4 for Ctrl (2 males, 2 females) and N = 5 for cKO (3 males and 2 females). Scale bar = 10 μm. **c.** Representative images of APC^{+} mature

oligodendrocytes in the CC of Ctrl or cKO brains at 3 days post-TBI. Arrows: APC^+ mature OLs. Scale bar = 10 μm. **d.** Colocalization of $Olig2^+$ with the APC^+ mature oligodendrocytes. **e.** Quantification of APC^+ mature oligodendrocytes in the CC of Ctrl or cKO brains at 1, 3, and 30 days post-TBI. * $p < 0.05$, ** $p < 0.01$, *** $p < 0.001$, **** $p < 0.0001$.

Figure 3

Selective deletion of microglial *Nhe1* reduced inflammatory responses in cKO mice at 3 days post-TBI.

a. Representative gating strategy of $CD11b^+CD45^{lo}$ microglia and $CD11b^+CD45^{hi}$ myeloid cells using flow cytometry. **b.** Percentages of the $CD11b^+CD45^{lo}$ microglia and $CD11b^+CD45^{hi}$ macrophage populations within live singlet cells of Ctrl or cKO brains at 3 days post-TBI. **c-d.** Expressions of pro- and anti-inflammatory markers within $CD11b^+CD45^{lo}$ or $CD11b^+CD45^{hi}$ populations. Data are mean ± SEM, N = 6 for Ctrl (3 males, 3 females) and N = 7 for cKO (4 male, 3 females). **e.** Representative images and quantification of $GFAP^+$ reactive astrocytes and $IBA1^+$ microglia/macrophages in the peri-lesion cortex of Ctrl or cKO brains at 3 days post-TBI. Scale bar = 20 μm. Data are mean ± SEM, N = 6 for Ctrl (3 males, 3 females) and N = 10 for cKO (6 males, 4 females). * $p < 0.05$, ** $p < 0.01$, *** $p < 0.001$, **** $p < 0.0001$.

Figure 4

Microglial *Nhe1* deletion alters pro- and anti-inflammatory transcriptome profiles in microglia/macrophages at 3 days post-TBI.

a. Bulk RNAseq of $CD11b^+$ microglia/myeloid cells isolated from CL and IL hemispheres of Ctrl and cKO mice at 3 days post-TBI. **b**. Unsupervised hierarchical clustering and heatmap illustration of up-and down-regulated genes. **c**. Venn diagram depicting differential gene expression; FDR q value ≤0.05, fold change of ≥ 1.2 or ≤ -1.2. **d**. Volcano plots illustrate the gene expression pattern (detected with log2 fold change of ≥1.2 and FDR q-value ≤ 0.05). **e.** Enrichment analysis showing significantly altered top canonical pathways using Ingenuity Pathway Analysis software. **f-g**. Scatter plots showing expression of Th1/Th2 pathway and pro- and anti-inflammatory genes presented as normalized counts. Data are mean ± SEM, N = 4 for Ctrl (all males) and N = 3 for cKO (all males). *$p < 0.05$, **$p < 0.01$, ***$p < 0.001$, ****$p < 0.0001$.

Figure 5

Post-TBI administration of selective NHE1 inhibitor HOE642 in C57BL/6 wild-type mice accelerated neurological function recovery.

a. Experimental protocol. Either Veh (2.5% DMSO in PBS) or HOE642 (0.15mg/kg) was administered twice per day from 1-7 days post-TBI in the C57BL/6J wild-type (WT) mice. **b.** Survival rate of Veh or HOE-treated mice at 1-30 days post-TBI. **c.** Adhesive contact and removal time of Veh and HOE-treated mice at 1-14 days after TBI. **d.** Foot fault test of the same cohort of mice in C. **e.** Y-maze test of the same cohort of mice in C at 30 days post-TBI. N = 7-11. Data are mean ± SEM. * $p < 0.05$, **** $p < 0.0001$, Veh. vs. HOE-treated groups.

Figure 6

Post-TBI administration of selective NHE1 inhibitor HOE642 in C57BL/6 wild-type mice showed neuroprotection and enhanced oligodendrogenesis.

a. Contusion volume of Veh or HOE-treated brains at 3 days post-TBI by MAP2 staining. Data are mean ± SEM. N = 5-6. **b.** Immunostaining of MAP2 and NeuN in the perilesion cortex of Veh or HOE-treated brains at 3 days post-TBI. Scale bar = 50 μm. **c.** Representative images and quantification of Olig2 colocalized with NG2, Ki67, Caspase-3, and H3K9me3 in CC at 3 days post-TBI. Arrows: colocalized cells. Scale bar = 10 μm. Data are mean ± SEM. N = 3-4. * $p < 0.05$, *** $p < 0.001$, **** $p < 0.0001$.

Figure 7

Increased white matter integrity in microglial *Nhe1* cKO and HOE642-treated mice at 30 days post-TBI.

a-b. Representative images of brains from rostral to caudal, and calculations of lesion volume and atrophy of T2 MRI of the *ex vivo* brains of Ctrl and cKO mice at 30 days post-TBI. **c-d.** Representative DTI diffusion encoded color (DEC) map and analysis of FA in the white matter tracts (CC and EC) of the same cohort of mice in a. Colors hues represent the principle orientation of the diffusion tensor (red = left/right, blue = dorsal/ventral, and green = rostral/caudal) with the intensity weighted by the FA. **e-f**. Representative images and calculations of lesion volume and atrophy of T2 MRI of the *ex vivo* brains of the Veh-control and HOE642-treated mice at 30 days post-TBI. **g-h.** Representative DTI DEC map and analysis of FA in the white matter tracts of the same cohort of mice in D. Data are mean ± SEM. N = 4. * $p < 0.05$, ** $p < 0.01$, *** $p < 0.001$, **** $p < 0.0001$.

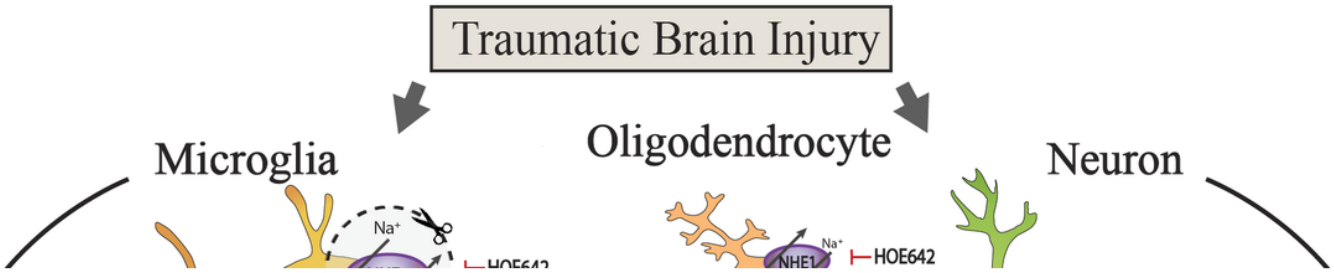

Figure 8

Schematic illustration of microglial NHE1 protein activation in white matter tissue damage/repair after TBI.

TBI triggers NHE1 activation in both microglia and neurons. Specific inhibition of NHE1 protein in microglia not only reduced acute contusion volume, but also significantly ameliorated inflammatory microenvironment, promoting restorative microglial function and myelination after TBI. These outcomes were recapitulated with administration of a potent NHE1 inhibitor HOE642 post-TBI. Taken together, these findings demonstrated that blocking NHE1 protein stimulates restorative microglial activation and oligodendrogenesis, which contributes to accelerated white matter repair and neurological function recovery after TBI.

Supplementary Files

This is a list of supplementary files associated with this preprint. Click to download.

- Songetalsupplementalfinal.docx